

M. WAKEDA¹
Y. SHIBUTANI^{1,2,✉}
S. OGATA³
J. PARK⁴

Multiple shear banding in a computational amorphous alloy model

¹ Department of Mechanical Engineering, Graduate School of Engineering, Osaka University, Yamadaoka, Suita, Osaka 565-0871, Japan
² Center of Atomic and Molecular Technologies, Graduate School of Engineering, Osaka University, Yamadaoka, Suita, Osaka 565-0871, Japan
³ Department of Mechanical Science and Bioengineering, Graduate School of Engineering Science, Osaka University, Machikaneyama, Toyonaka, Osaka 560-8531, Japan
⁴ POSCO, Technical Research Laboratories, Korea

Received: 26 October 2007 / Accepted: 10 December 2007
Published online: 15 February 2008 • © Springer-Verlag 2008

ABSTRACT The strain localized phenomenon, so called shear bands (SBs), in an amorphous alloy have received a lot of attention in recent years. In this study, we microscopically investigated the nature and dynamics of multiple SBs using molecular dynamics model. In the SB region, intense shear-induced structural change occurred, typified by the annihilation of pentagonal short-range order, and significant localized heating accompanied with the SB propagation was observed. Moreover, a large number of fine SBs operated simultaneously at a high strain rate, whereas, only a few SBs appeared and propagated abruptly at a low strain rate. These results were discussed with respect to brittle/ductile deformation of bulk metallic glasses.

PACS 31.15.xv; 62.20.F-; 81.05.Kf

1 Introduction

At ambient temperature, conventional amorphous metals and also bulk metallic glasses (BMGs), which have high glass forming ability (GFA) and hence can be obtained in large-sized bulk form [1], exhibit a noticeably large elastic limit of 2%. However, due to localized inhomogeneous deformation, they fracture shortly after the onset of yielding [2]. Such abrupt and unpredictable fracture limits the applications of BMGs as engineering materials, in spite of their excellent intrinsic mechanical properties, such as high yield strength and high fracture toughness. For the past thirty years, a number of studies have focused on the fracture behavior, specifically on the localized deformation, the so-called shear band (SB) [2–5]. According to laboratory-based experiments, plastic deformation of BMGs at low temperatures is concentrated in narrow bands with widths of 10–20 nm [6]. Cracking is initiated and propagated at the location of the SB leading to catastrophic fracture.

Recently, the positive beneficial role of high density SBs on ductility has been reported in a number of experiments, which include the following:

- (i) a large density of pre-introduced multiple shear bands (MSBs) by cold rolling increased the plastic elongation [7],
- (ii) BMGs with dispersed nanocrystalline particles exhibited high ductility since the particles promoted the formation of MSBs and obstructed SB propagation [8], and
- (iii) the influence of interactions and intersections between SBs on the ductility was also reported [9, 10].

In experiments, however, an understanding of shear banding is generally based on observations of post-deformed specimens, and it is difficult to reveal the SB nucleation and propagation processes. Some significant questions regarding the nature and dynamics of shear banding are still controversial. These include:

- (i) where and how does SB nucleate and propagate?
- (ii) what factors contribute to softening in the SB region, heating, packing density, or other effects [11–13]?
- (iii) And how does the loading rate affect MSB dynamics and macroscopic plasticity [14–17]?

To understand the nature of shear banding and brittle/ductile deformation of BMGs, molecular dynamics (MD) simulation, which can describe the dynamics of individual atoms, is expected to serve as a useful reference. In recent years, a series of MD studies, focusing on localized phenomena in BMGs, have been conducted, including structural transformation and localization under nanoindentation [18], single SB analysis under compression [19], microscopic characterization of SBs by bond length, potential energy, etc. [20], observation of parallel SBs under simple shear [21], and SB propagation criterion [5].

In the present MD study, our first aim is to understand the nature and dynamics of SBs from an atomistic viewpoint. The time evolution of SB nucleation/propagation process and corresponding macroscopic stress behavior are shown in Sect. 3.1, and strain localization and softening processes are investigated with respect to the local geometric structure and concentrated heating in Sect. 3.2. In addition, in Sect. 3.3, the strain rate effect on dynamics of SBs is investigated. Finally, in Sect. 4, we summarize the results and discuss high strain

✉ Fax: +81-06-6879-4121, E-mail: sicutani@mech.eng.osaka-u.ac.jp

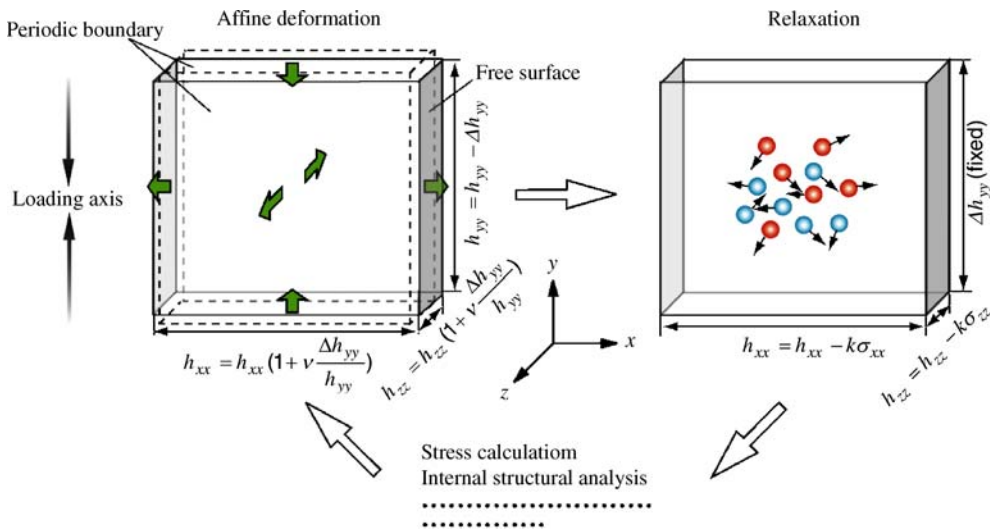


FIGURE 1 Schematic illustrations explaining the procedure of uniaxial compressive loading employed in this study

rate-induced macroscopic plasticity in BMGs related to the simultaneous operation of MSBs.

2 Analysis model and simulation method

We constructed a binary amorphous alloy model via a melt-quench process [22]. The applied interatomic potentials were simple Lennard–Jones 4-8 [23], the parameters for which were determined to satisfy the lattice sizes and elastic constants of Cu and Zr *fcc* crystals. Therefore, our amorphous model represented here is the Cu–Zr system, which is one of the most common binary amorphous metals. The external pressure during the melt-quenching process was maintained at zero by the Parrinello–Rahman ensemble [24], and the temperature of the whole cell was controlled by scaling the velocity of each atom. The number of Cu and Zr atoms, cell size and density of the constructed model are represented in Table 1. The amorphous structure was confirmed by the analysis of the radial distribution function (RDF) and Voronoi polyhedron. In addition, the first peaks of RDF and the density agreed well with those obtained experimentally [22].

To explore the strain localization phenomenon, we performed uniaxial compressive simulations by restricting atomic displacements in two dimensions. Under uniaxial loading, MD models generally show homogeneous plastic deformation and yield without strain localization [26, 27], since MD systems have spatiotemporal limits which reduce the model scale and increase the loading rate. The two-dimensional constraint applied in this study reduces the spatiotemporal scale of the localized phenomena, thus it has a positive influence on the generation of MSBs in amorphous MD models. The present uniaxial loading procedure is shown in Fig. 1. We ap-

plied periodic boundary conditions to the *y* (loading axis) and *z* directions but free boundary conditions only to the *x* direction, and then sufficiently relaxed the atomic configuration and model cell during 20 ps (equivalent to 20 000 MD steps) to obtain the equilibrium state. Following the relaxation, uniaxial loading was implemented by repeating the two processes. First, an affine deformation was applied to the model cell by decreasing in the *y* direction, while increasing in the *x* and *z* directions taking into account the transverse strain (temporal Poisson's ratio set to 0.4). Then, the atomic configurations were allowed to relax within the *x*–*y* plane, i.e. the *z* coordination was fixed. After affine deformation, σ_{xx} and σ_{zz} had non-zero values, since the transverse strains were determined based on the approximate Poisson's ratio. Therefore, during the relaxation, *x* and *z* dimensions of the model cell were continually controlled by feeding back the stresses of σ_{xx} , σ_{zz} to maintain the uniaxial stress state ($\sigma_{xx} = \sigma_{zz} = 0$). The strain rates adopted here were set to $5 \times 10^8 \text{ s}^{-1}$, $5 \times 10^9 \text{ s}^{-1}$, and $5 \times 10^{10} \text{ s}^{-1}$, and, through the loading, the temperature was not artificially controlled from the initial setting T_0 of 50 K.

Number of atoms	500 000	Cu: 285 000 Zr: 215 000
Size of cell	$69.8 \times 69.4 \times 1.75 \text{ nm}^3$	
Density	7.34 g/cm^3	

TABLE 1 Total number of atoms, cell size, and density of the constructed model. The experimentally obtained density of 7.38 g/cm^3 [25] agrees well with that of our computational model

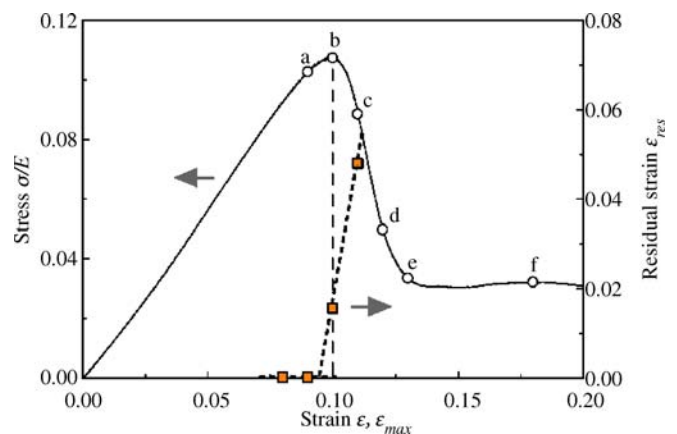


FIGURE 2 The relationship between true stress σ (normalized by Young's modulus $E = 111.4 \text{ GPa}$) and nominal strain ϵ at an intermediate strain rate of $5 \times 10^9 \text{ s}^{-1}$. The four square symbols represent the residual strain ϵ_{res} as a function of maximum applied strain ϵ_{max} ($= 0.08, 0.09, 0.10, \text{ and } 0.11$). The six open circles a–f correspond to the snapshots in Fig. 3

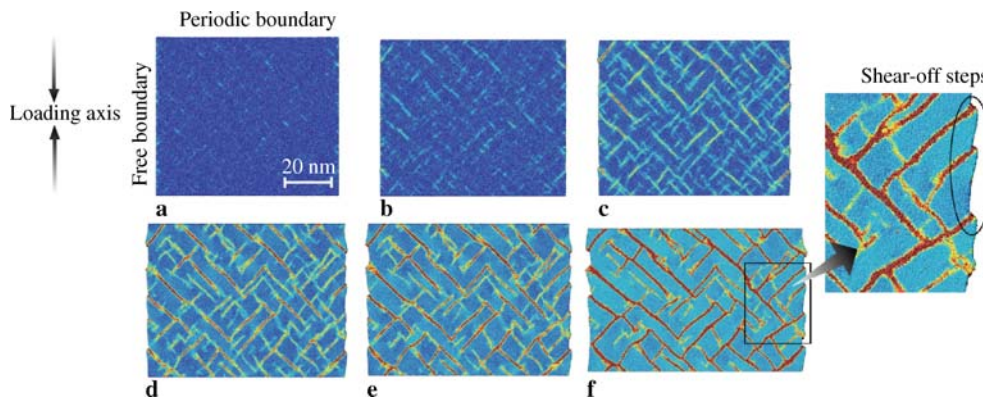


FIGURE 3 A series of snapshots from the uniaxial compressive process at $\varepsilon =$ (a) 0.09, (b) 0.10, (c) 0.11, (d) 0.12, (e) 0.13, and (f) 0.18. We also employed another evaluation scheme, the so-called “atomic strain” (originally defined in [29] and applied to the GFA of amorphous alloys in [30]), and confirmed that the visualized snapshots omitted here were very similar to those in Fig. 3

3 Simulation results

3.1 SBs nucleation and propagation process

The stress vs. strain relationship during the uniaxial compressive process at an intermediate strain rate of $5 \times 10^9 \text{ s}^{-1}$ is shown in Fig. 2. In the early stage of deformation, the stress curve almost linearly increases with increasing strain, and has a peak at around $\varepsilon = 0.10$. In order to determine the yield point via the strain recovery method [28], we also performed loading–unloading simulations, and the residual strains ε_{res} were represented as a function of the applied maximum strain ε_{max} . The existence of residual strain after unloading indicates that the plastic deformation starts shortly before the maximum stress.

Figure 3 shows a series of snapshots at $\varepsilon = 0.09, 0.10, 0.11, 0.12, 0.13,$ and 0.18 , which are indicated by points a–f in Fig. 2. In the figures, each atom is colored by the local rearrangement evaluation scheme defined here. In crystal structures, dislocations can be easily visualized by the excess potential energy of the atoms. Amorphous metals, however, have an inherent inhomogeneous macroscopic structure, and thus it is difficult to identify regions which deform plastically. In this work, the extent of local rearrangement was quantified as follows. For the initial configuration, the nearest neighbor atoms were registered for each atom (the neighborhood was defined by the cut-off radii of the applied potentials). Then, the relative atomic displacements of the neighbor atoms were calculated based on the normalized atomic coordinates so as to eliminate global applied strain.

At $\varepsilon = 0.10$, MSBs simultaneously emerge at the free surface and also inside the model. Drastic stress decrement is then induced by the MSB propagation. In the present model, most SBs are straight, and approximately lie along the maximum shear stress direction. It is interesting to note that, shortly after initiation, SBs are found to be oriented several degrees smaller than 45° with respect to the loading axis. This deviation implies that the SB propagation in the MD model follows the Mohr–Coulomb criterion and not the von Mises criterion, and is consistent with several experimental observations [2, 14, 16], wherein the angle between SBs and loading axis is larger than 45° under tension, and is smaller than 45° under compression. As shown in the snapshots, SB propagation is blocked by other crossing “active” SBs (which are not cooled down and are still soft), therefore the stress drop is completed at around $\varepsilon = 0.13$. For deformation beyond the

point, there is no more SB generation. Alternatively, concentrated slip occurs in the existing large SBs, resulting in prominent shear-off steps on the free surface.

3.2 Structural and thermal features of SB

In order to understand the local geometric structures inside and outside the SBs, we applied the Voronoi analysis determined by the atomic configuration between the centered and the nearest neighbor atoms. It has been indicated that the amorphous structure is distinguished from the liquid state by the high content of nonperiodic pentagonal short-range order (SRO): at the transition from liquid to amorphous phase, the pentagonal SRO increases and, vice versa, other SRO such as tetragonal and hexagonal structure decrease [22, 31, 32]. The density distribution of the Voronoi pentagons at $\varepsilon = 0.13$ is shown in Fig. 4a. Inside the SB regions, a reduction in pentagonal short-range structure is found, indicating that localized shear deformation accompanies the disordering, typified by the annihilation of amorphous specific SRO. In the previous study [22], we pointed out that the pentagonal SRO had dense packing configurations, and is therefore closely related to the free volume content, which

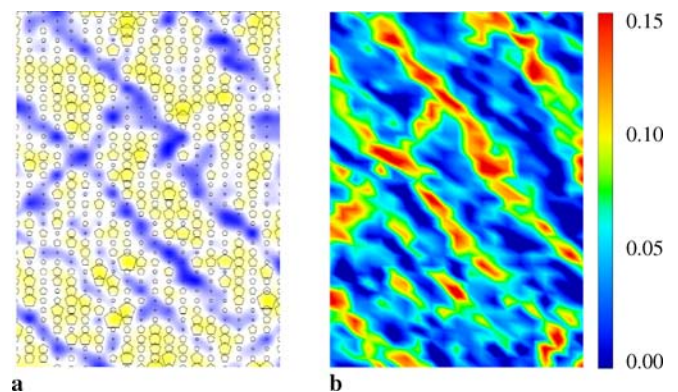


FIGURE 4 Distribution of (a) pentagonal SRO and (b) free volume around SBs at $\varepsilon = 0.13$. In (a), the number density distribution of pentagons is represented by the size of the *pentagonal symbols* and also by the color map. Details of the calculation procedure are mentioned in our previous study [22]. The free volume of each atom shown in (b) is calculated from the composition-related equation $V/(0.57V_{\text{Cu}} + 0.43V_{\text{Zr}})$, where V is a volume of a Voronoi cluster, and V_{Cu} and V_{Zr} are atomic volumes of Cu and Zr crystals obtained from one-component models

was a critical factor in the analysis of the deformation behavior of amorphous metals [22, 33]. Here, we have estimated the free volume based on the volume increment from the crystalline state, as in [22], and the distribution around the SBs is shown in Fig. 4b. The alteration of SRO induces a noticeable free volume increment at the location of the SBs; the low density state at the strain localized regions is consistent with other MD analyses [5, 20]. As indicated by the early constitutive model of plastic deformation [12], the slight change in packing density has enormous influence on the viscosity, since the high free volume structure allows atoms to easily jump to empty sites under shear stress.

In laboratory-based experiments, it is difficult to clarify SB-specific local configurations due to the extremely disordered atomic structure. However, the present calculations intrinsically relate to some experimental facts:

- (i) the SB regions had preferential etching susceptibility, indicating a change in SRO [3],
- (ii) atomic disorder increment in the SB region has been observed by high-resolution transmission electron microscopy [34],
- (iii) the increase in the free volume at SBs was indicated by early work [35, 36], and also in a recent report using positron annihilation spectroscopy [13].

In Fig. 5, we represent the average temperature rise for the whole model and the average potential energy per atom during the loading process. For the potential energy, two kinds of values are plotted; the average for the whole model, and the average of the small region having no SBs (containing 3500 atoms). In the present calculation, a temperature control scheme was not employed, therefore applied work was essentially converted into potential or thermal energies without any energy dissipation. In elastic deformation, applied work is almost accumulated as elastic strain energy and thus there is no temperature rise. Then, the release of elastic strain energy in a no SB region and an increment in temperature are simultaneously observed at the start of strain localization at $\varepsilon = 0.10$. The inset in Fig. 5 shows a snapshot showing the temperature distribution at $\varepsilon = 0.11$. Local heating is highly concen-

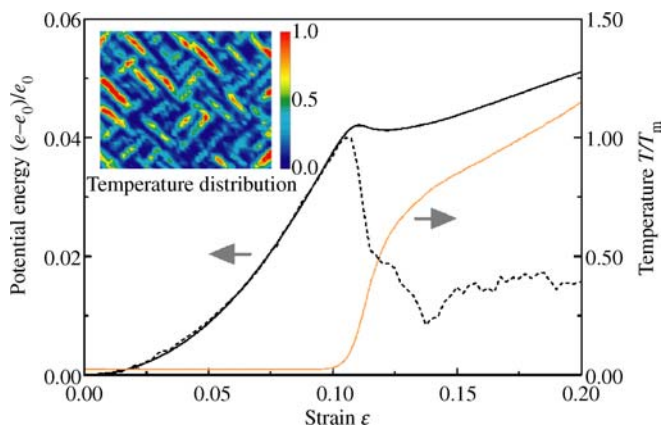


FIGURE 5 Average potential energy per atom e and average temperature of the whole model T vs. the nominal strain (e_0 represents the average potential energy at $\varepsilon = 0$, and T_m represents the melting temperature obtained from heating simulation under the same 2D constraint). The *embedded image* represents a distribution of T/T_m at $\varepsilon = 0.11$

trated in the SB region, specifically in the dominant bands with larger shear displacement. The temperature rise may be caused by the friction of atoms at the intensely sheared area, and is proportional to the magnitude of shear displacement. Therefore, significant heating at mature SBs finally induces fatal lowering of local viscosity.

3.3 Effect of loading rate on MSBs dynamics

Stress vs. strain relationships at a lower strain rate of $5 \times 10^8 \text{ s}^{-1}$ and a higher rate of $5 \times 10^{10} \text{ s}^{-1}$ are represented in Fig. 6. The stress-strain curves initially show the same behavior, however, the starting point of plastic deformation and the flow stress behavior largely depend on the strain rate. The elastic limit and the maximum stress increase with increasing strain rate; thus, the extremely large elastic limits of 9%–12% that were observed in this study may be caused by unrealistic applied strain rates, which are several orders of magnitude larger than those in experimental studies. At a lower strain rate, the stress drops almost perpendicularly at the start of plastic deformation, while stress decreases more slowly at a higher rate. Snapshots of the lower strain rate (at $\varepsilon = 0.10$) and higher strain rate (at $\varepsilon = 0.20$) are shown in the insets in Fig. 6. At the lower rate, a few SBs initiate and abruptly propagate. In this case, plastic deformations are highly localized in the region of a few SBs, therefore the large shear displacement accompanying a significant temperature rise is observed. However, at a higher strain rate, a large number of fine SBs appear at the same instant, promoting homogeneous strain relaxation. Thus, in the higher strain rate case, we could not observe clear shear-off steps on the free surface.

The present relation between strain rate and the number of SBs is consistent with experimental observations of post-fracture specimens [14, 15, 17], wherein only a single SB leading to a final crack or secondary SBs near the fracture surface are observed at a lower strain rate, while a large number of SBs can be seen in the whole volume of the samples at a higher strain rate. The present MD observations provide an explanation for the dynamics of SBs. At a low strain rate, there

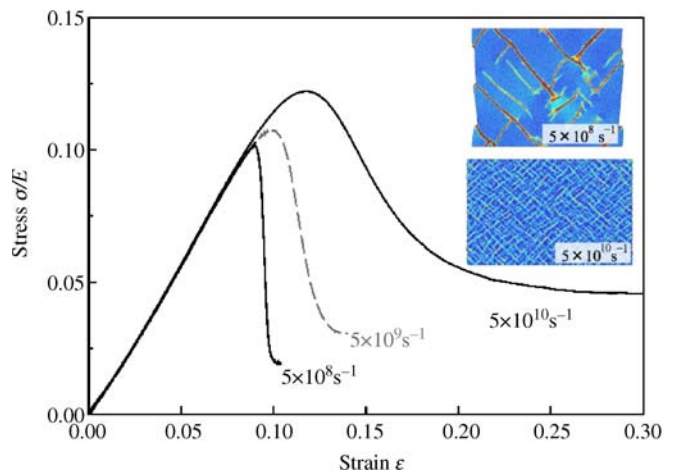


FIGURE 6 Stress vs. strain curves for a lower strain rate ($5 \times 10^8 \text{ s}^{-1}$), a higher strain rate ($5 \times 10^{10} \text{ s}^{-1}$), and, for comparison, an intermediate strain rate. The *inset* figures represent snapshots of the lower rate at $\varepsilon = 0.10$ and the higher strain rate at $\varepsilon = 0.20$, respectively

is sufficient time for the initially generated SBs to propagate. However, a high strain rate cannot provide time for stress relaxation at the initial SBs, hence a high stress state generates other new SBs all over the model.

4 Concluding remarks

In the literature, MD simulations were performed to investigate the nature and dynamics of strain localized phenomena, which is a crucial factor for brittle/ductile deformation of BMGs. In the SB region, intense shear induces structural change, typified by the annihilation of pentagonal SRO, results in the generation of a low packing state, the so-called free volume. The plastic deformation of amorphous metals is expected to be caused by individual atomic jumps to empty sites [33], therefore applied strain is highly localized in the free volume structure, promoting the formation of shear banding. In addition, the propagation of SBs is accompanied by a concentrated temperature rise. Evidence of melting on the fracture surface has been observed in recent experimental studies [2, 10]. The low viscosity derived from the free volume structure as well as the significant temperature rise is expected to be a direct cause of final fracture in the SB region.

However, the relation between the MSB dynamics and loading rate was also investigated; at a higher strain rate, a large number of fine SBs simultaneously appear, while at a lower strain rate, a few SBs initiate and abruptly propagate. It was reported just recently that the deformation mode of BMGs suddenly transitioned from brittle fracture to ductile deformation involving MSB operation, when the applied strain rate exceeded some critical value [15, 17]. However, several studies have reported contradictory experimental results [14, 16], and the loading rate dependence of SB behavior and brittle/ductile deformation are still controversial. The present observation of the dynamics of SBs supports the positive influence of high strain rate on the generation of MSBs: a sufficiently large strain rate prevents stress relaxation at a single SB, and results in the generation of a number of SBs all over the model. High density MSBs enhances macroscopic ductility, since it

- (i) impedes sudden SB propagation due to the interactions [8, 9] and
- (ii) promotes homogeneous strain relaxation [7].

Basically, an SB itself has fatal low viscosity leading to brittle fracture, as shown in a number of experimental reports. Therefore, in order to improve the ductility of BMGs, it is cru-

cial to generate high density MSBs before a single mature SB induces catastrophic fracture.

ACKNOWLEDGEMENTS One of the authors, Y.S., gratefully acknowledges support from the Ministry of Education, Culture, Sports, Science and Technology in Japan, for a Grant-in-Aid for Scientific Research on Priority Areas (15074214), and M.W. acknowledges support from a Grant-in-Aid for JSPS Fellows.

REFERENCES

- 1 A. Inoue, *Mater. Trans. JIM* **36**, 866 (1995)
- 2 Z.F. Zhang, J. Eckert, L. Schultz, *Acta Mater.* **51**, 1167 (2003)
- 3 C.A. Pampillo, *Scr. Metall.* **6**, 915 (1972)
- 4 K.D. Krishnanand, R.W. Cahn, *Scr. Metall.* **9**, 1259 (1975)
- 5 F. Shimizu, S. Ogata, J. Li, *Acta Mater.* **54**, 4293 (2006)
- 6 E. Pekarskaya, C.P. Kim, W.L. Johnson, *J. Mater. Res.* **16**, 2513 (2001)
- 7 Y. Yokoyama, K. Yamano, K. Fukaura, H. Sunada, A. Inoue, *Scripta Mater.* **44**, 1529 (2001)
- 8 Y.K. Xu, H. Ma, J. Xu, E. Ma, *Acta Mater.* **53**, 1857 (2005)
- 9 K.F. Yao, F. Ruan, Y.Q. Yang, N. Chen, *Appl. Phys. Lett.* **88**, 122106 (2006)
- 10 J. Eckert, J. Das, K.B. Kim, F. Baier, M.B. Tang, W.H. Wang, Z.F. Zhang, *Intermetallics* **14**, 876 (2006)
- 11 W.J. Wright, R.B. Schwarz, W.D. Nix, *Mater. Sci. Eng. A* **319–321**, 229 (2001)
- 12 P.S. Steif, F. Spaepen, J.W. Hutchinson, *Acta Metall.* **30**, 447 (1982)
- 13 K.M. Flores, D. Suh, R.H. Dauskardt, P. Asoka-Kumar, P.A. Sterne, R.H. Howell, *J. Mater. Res.* **17**, 1153 (2002)
- 14 T. Mukai, T.G. Nieh, Y. Kawamura, A. Inoue, K. Higashi, *Scripta Mater.* **46**, 43 (2002)
- 15 A.V. Sergueeva, N.A. Mara, D.J. Branagan, A.K. Mukherjee, *Scripta Mater.* **50**, 1303 (2004)
- 16 L.F. Liu, L.H. Dai, Y.L. Bai, B.C. Wei, G.S. Yu, *Intermetallics* **13**, 827 (2005)
- 17 A.V. Sergueeva, N.A. Mara, J.D. Kuntz, E.J. Lavernia, A.K. Mukherjee, *Philos. Mag.* **85**, 2671 (2005)
- 18 Y. Shi, M.L. Falk, *Appl. Phys. Lett.* **86**, 011914 (2005)
- 19 Y. Shi, M.L. Falk, *Phys. Rev. B* **73**, 214201 (2006)
- 20 Q.K. Li, M. Li, *Appl. Phys. Lett.* **88**, 241903 (2006)
- 21 S. Ogata, F. Shimizu, J. Li, M. Wakeda, Y. Shibutani, *Intermetallics* **14**, 1033 (2006)
- 22 M. Wakeda, Y. Shibutani, S. Ogata, J. Park, *Intermetallics* **15**, 139 (2007)
- 23 S. Kobayashi, K. Maeda, S. Takeuchi, *Acta Metall.* **28**, 1641 (1980)
- 24 M. Parrinello, A. Rahman, *J. Appl. Phys.* **52**, 7182 (1981)
- 25 Y. Waseda, T. Masumoto, *Z. Phys. B* **21**, 235 (1975)
- 26 K. Nakatani, H. Kitagawa, A. Nakatani, *J. Soc. Mater. Sci. Japan* **46**, 244 (1997)
- 27 A.C. Lund, C.A. Schuh, *Acta Mater.* **51**, 5399 (2003)
- 28 R. Quinson, J. Perez, M. Rink, A. Pavan, *J. Mater. Sci.* **32**, 1371 (1997)
- 29 P.H. Mott, A.S. Argon, U.W. Suter, *J. Comput. Phys.* **101**, 140 (1992)
- 30 J. Park, Y. Shibutani, S. Ogata, M. Wakeda, *Mater. Trans.* **46**, 2848 (2005)
- 31 H. Jónsson, H.C. Andersen, *Phys. Rev. Lett.* **60**, 2295 (1988)
- 32 D.W. Qi, S. Wang, *Phys. Rev. B* **44**, 884 (1991)
- 33 F. Spaepen, *Acta Metall.* **25**, 407 (1977)
- 34 J. Li, Z.L. Wang, T.C. Hufnagel, *Phys. Rev. B* **65**, 144201 (2002)
- 35 P.E. Donovan, W.M. Stobbs, *Acta Metall.* **29**, 1419 (1981)
- 36 A.S. Argon, J. Megusar, N.J. Grant, *Scripta Metall.* **19**, 591 (1985)